Atomic-Scale Insights into the Low-Temperature Oxidation of Methanol over a Single-Atom Pt_1-Co_3O_4 Catalyst

Zeyu Jiang, Xiangbo Feng, Jianlin Deng, Chi He, Mark Douthwaite, Yanke Yu, Jian Liu,* Zhengping Hao, and Zhen Zhao*

Heterogeneous catalysts with single-atom active sites offer a means of expanding the industrial application of noble metal catalysts. Herein, an atomically dispersed Pt_1-Co_3O_4 catalyst is presented, which exhibits an exceptionally high efficiency for the total oxidation of methanol. Experimental and theoretical investigations indicate that this catalyst consists of Pt sites with a large proportion of occupied high electronic states. These sites possess a strong affinity for inactive Co^{2+} sites and anchor over the surface of (111) crystal plane, which increases the metal–support interaction of the Pt_1-Co_3O_4 material and accelerates the rate of oxygen vacancies regeneration. In turn, this is determined to promote the coadsorption of the probe methanol molecule and O_2. Density functional theory calculations confirm that the electron transfer over the oxygen vacancies reduces both the methanol adsorption energy and activation barriers for methanol oxidation, which is proposed to significantly enhance the dissociation of the C H bond in the methanol decomposition reaction. This investigation serves as a solid foundation for characterizing and understanding single-atom catalysts for heterogeneous oxidation reactions.

1. Introduction

Reducing the emission of volatile organic compounds (VOCs) is one of the biggest challenges facing the chemical industry in the 21st century. Many VOCs are considered to pose signifi-cant health hazards (carcinogenic, mutagenic, and teratogenic properties) and linked with various environmental hazards, such as photochemical smog and ozone depletion.[1] Methanol, as an oxygenated volatile organic compound (OVOC), is widely used in numerous industrial applications.[2] Catalytic oxidation over supported noble metal catalysts has emerged as a promising method for these compounds removal from industrial waste streams, ascribing to their high specific activity, resistance to deactivation, and ability to be regenerated.[3] In our previous works, we determined that Pt-based catalysts are highly active for the low-temperature decomposition of methyl ethyl ketone.[4] The economic limitations associated with the industrial application of these catalysts have, however, reduced their widespread utilization.[5] As such, an abun-dance of researches are currently ongoing to tackle these challenges.[6]

Single-atom catalysts (SACs) offer a means of reducing the costs associated with the preparation and utilization of noble metal catalysts.[7] The recent expansion to research in this area will undoubtedly assist with the development of sustainable catalytic technologies for a host of important industrial applications.[7c,8] Single-atom Pt-based cata-lysts have already been applied to various heterogeneous oxi-dation reactions, particularly for CO oxidation.[9] Qiao et al.[9a] designed a catalyst consisting of isolated single Pt atoms, which were anchored to the surface of iron oxide nanocrystallites.

Z. Y. Jiang, Prof. C. He
State Key Laboratory of Multiphase Flow in Power Engineering School of Energy and Power Engineering
Xi'an Jiaotong University
Xi'an 710049, Shaanxi, P. R. China
E-mail: chi_he@xjtu.edu.cn

Dr. X. B. Feng
Shaanxi Engineering Research Center of Controllable Neutron Source Xijing University
Xi'an 710123, Shaanxi, P. R. China

J. L. Deng, Prof. J. Liu, Prof. Z. Zhao
State Key Laboratory of Heavy Oil Processing China University of Petroleum
Beijing 102249, P. R. China
E-mail: liujian@cup.edu.cn

Prof. C. He, Prof. Z. P. Hao
National Engineering Laboratory for VOCs Pollution Control Material and Technology
University of Chinese Academy of Sciences Beijing 101408, P. R. China

Dr. M. Douthwaite
Cardiff Catalysis Institute
School of Chemistry
Cardiff University
Main Building, Park Place, Cardiff CF10 3AT, UK Dr. Y. K. Yu
Department of Chemical Engineering
Columbia University
NY 10027, USA

Prof. Z. Zhao
Institute of Catalysis for Energy and Environment Shenyang Normal University
Shenyang 110034, P. R. China

When tested for CO oxidation, this SAC exhibited a turnover frequency H2–3 times higher than a corresponding Pt/Fe_2O_3 catalyst (with sub-nanometer Pt particles) and remained stable for up to 300 min.[9a] The inherent stability of single-site Pt catalysts for CO oxidation was further demonstrated by Zhang et al.,[9d] who determined that there was no observable deactivation over 60 sequential cycles when operating at temperatures between 100 and 400 °C. The excellent stability of this catalyst was attrib-uted to firmly anchored Pt atoms on the internal surface of the mesoporous Al_2O_3 support, which were proposed to be stabilized by coordinate unsaturated pentahedral Al^{3+} centers.[9d]

Regrettably, there are only limited examples for the use of SACs in the oxidation of VOCs.[10] One example was, how-ever, presented by Tang and co-workers,[11] who reported that a single-atom Ag-HMO catalyst (HMO: hollandite manganese oxide) was highly active in the oxidation of formaldehyde. The studies revealed that subtle changes in the support material could lead to electronic perturbations in the single-atom sites, which had a profound effect on the intrinsic reactivity of the cat-alyst. This was a consequence of changes in the silver atoms 4d electronic state, resulting in an increasing of both the metal– support interaction and reducibility of the catalyst.[11]

It is known that the activity, selectivity, and stability of SACs can be tuned by modifying the interactions between the anchored atoms and support surfaces.[12] The geometric location of these metal atoms on the surface of support is considered to impact how strongly the atoms interact with the support.[12b] The isolated single metal atoms, which are consid-ered to anchor over cationic vacancies/equivalent cationic posi-tions or to other surface defects on the support, are recognized as the active centers in these catalytic systems.[12] We therefore proposed that developing a greater understanding of how SACs affect oxidative reaction mechanism is paramount for their application as catalysts for the removal of VOCs.

As such, we began by synthesizing a highly oxygen-deficient single-atom Pt_1-Co_3O_4 catalyst via a facile one step method. A detailed description of the geometric and electronic structure of this catalyst and its role in the oxidation of methanol was established by conducting a series of experimental and theo-retical studies. A link in the structure and the origin of catalytic property was also investigated to demonstrate the excellent per-formance our single-atom Pt_1-Co_3O_4 catalyst in methanol total oxidation reactions.

2. Results and Discussion

2.1. Determination and Modeling of Single-Atom Sites

Herein, we aimed to promote the application of single-atom cata-lysts in VOC destruction. As such, we synthesized the Pt_1-Co_3O_4 catalyst over which the Pt atoms are anchored on the surface defects of Co_3O_4 due to the existence of inactive Co^{2+} species. During the coprecipitation process, the Pt atoms are inclined to occupy the inactive Co^{2+} sites and anchor over the surface of (111) crystal plane through metal–support interaction.[13] The exposed (111) facet of Co_3O_4 support consisted of queued Co and O atoms in isolated lines (**Figure 1**a). This was also sub-sequently confirmed to be the most stable Co_3O_4 conformation by theoretical calculations (Figure S1, Supporting Information). On this surface, two types of threefold-coordinate oxygen atoms (O_a and O_b) are exposed; O_a has three Co^{3+} ions as nearest neighbors, whereas O_b atoms are bound to one Co^{2+} ion and two Co^{3+} ions. Upon impregnation with chloroplatinic acid, the Pt nanoparticles (yellow circles) with around 0.5–3.1 nm particle size were supported on the Co_3O_4 (111) plane surface, which are highlighted in Figure 1b and Figure S2 (Supporting Informa-tion). No Pt nanoparticles could be observed from high-resolu-tion transmission electron microscopy- (HRTEM) images of the Pt_1-Co_3O_4 catalyst (Figure 1c and Figure S3, Supporting Infor-mation) and the intraplanar spacing (*d* values) were measured to be H0.45 nm, in good consistence with that of the exposed (111) crystal plane of the Co_3O_4 sample.[14] The fast Fourier transformation (FFT) of exposed facet is in well agreement with the standard Co_3O_4 (111) crystal plane.[13] In addition, as shown in Figure S4 (Supporting Information), no changes have occurred of FFT patterns between Co_3O_4 and single-atom Pt_1-Co_3O_4 materials, which indicates that the single-atom Pt sites are anchored over the surface of Co_3O_4 supports and the exist-ence of single atoms has a negligible effect on (111) crystal plane. In addition, the content of Pt detected by inductively coupled plasma optical emission spectrometry (ICP-OES) is similar to that determined by X-ray photoelectron spectroscopy (XPS) and X-ray fluorescence (XRF) methods (Table S1, Sup-porting Information), which confirms that the Pt active sites are almost located at the surface of support. Models for the opti-mized structure of the single-atom Pt_1-Co_3O_4 catalyst were sub-sequently proposed through considering all possible synergistic states (Figure 1d–f). Previously, aberration-corrected high-angle annular dark-field (HAADF) microcopy has been used to deter-mine the presence of heavy metals in SACs.[15] Upon utilization of this technique to probe the Pt_1-Co_3O_4 catalyst (Figure 1g–j), the presence of individual uniformly dispersed Pt atoms was observed. Extensive examination of additional catalytic regions in the sample confirmed that only Pt single atoms are present in the sample (Figure S5, Supporting Information).

Infrared (IR) spectrometry utilizing CO as the probe mole- cule is a fast and convenient characterization method to dif-ferentiate between metallic single atoms and nanoparticles.[16] When investigating Pt-containing catalysts, it can also be used to acquire information regarding the geometric configuration of the Pt centers.[16] No CO adsorption peak can be detected over the Co_3O_4 sample. In contrast, two CO adsorption bands pre-sented in the IR spectrum of the Pt_1-Co_3O_4 catalyst (Figure 1k). The adsorption bands centered at 2116 and 2029 cm^{-1} at room temperature correspond to the adsorption of CO over a single Pt atom and the asymmetric stretching vibrations of CO in the $Pt(CO)_2$ gem-dicarbonyl species on single Pt atoms, respectively.[16] With the Pt/Co_3O_4 catalyst however, only one peak can be observed at 2089 cm^{-1}, characteristic of linear CO adsorption over metallic Pt nanoparticles.[16a,b] To investigate how the adsorbed CO species on the surface of the Pt_1-Co_3O_4 catalyst was affected by exposure temperature, some additional IR experiments were conducted, and the results of which are displayed in Figure 1l. Interestingly, the intensity of the bands almost remain unchanged as the temperature increased in this experiment, indicating that the quantity of Pt active sites in the sample remained stable in temperature range 25–100 °C.

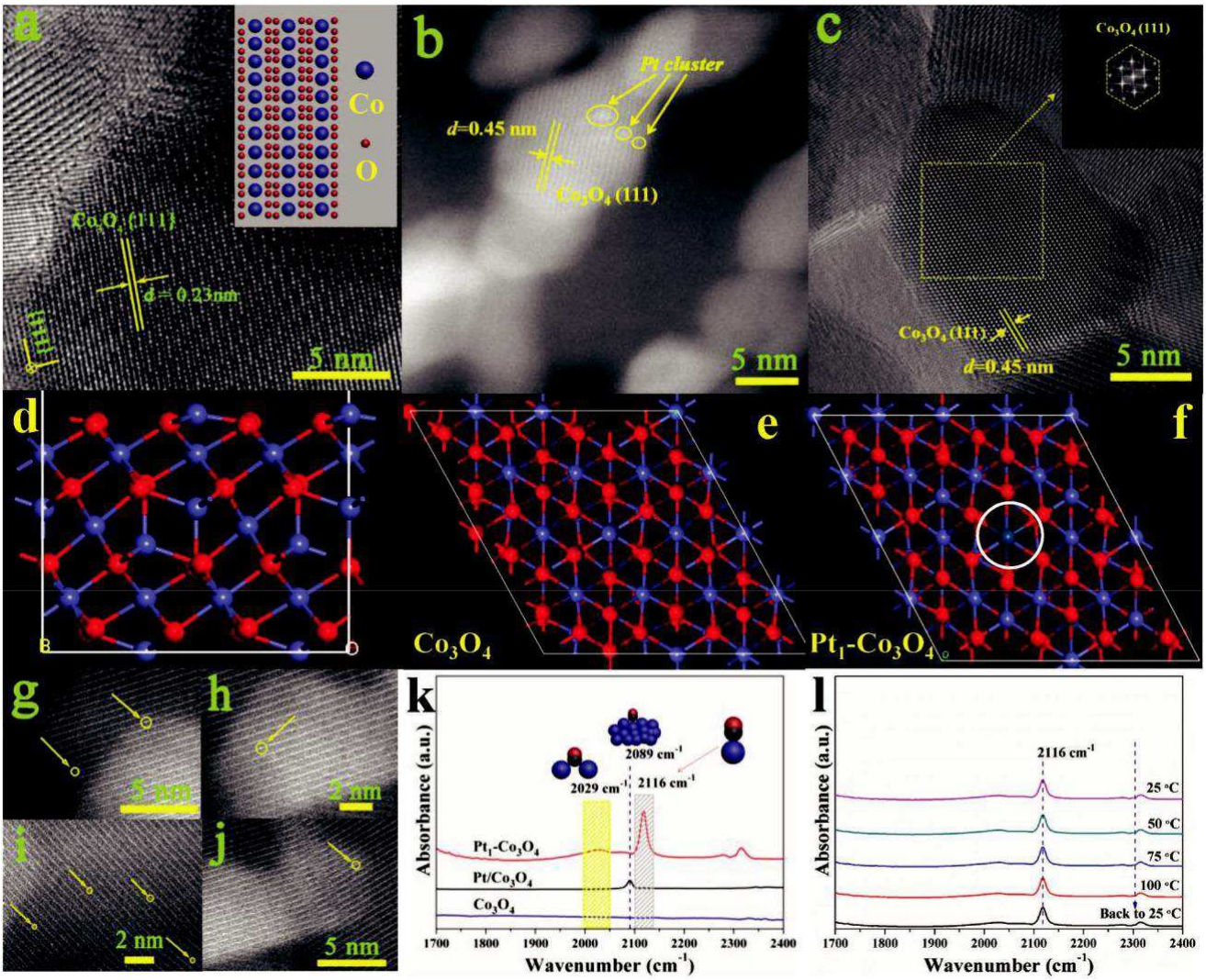

Figure 1. a–c) HRTEM images of Co_3O_4, Pt/Co_3O_4, and Pt_1-Co_3O_4 samples; d–f) Stable structure models optimized by theoretical calculations; g–j) Aberration-corrected HAADF-STEM images of Pt_1-Co_3O_4 material; k) In situ FTIR spectra of CO adsorption over prepared samples; l) Temperature-dependent CO adsorption over Pt_1-Co_3O_4 catalyst.

2.2. Determination of Electronic Structure and Defect Sites

Understanding the electronic structure of elemental com-ponents in a SAC is the most important challenge, which is fundamental for leading to the structure–activity correlations.[11] Representative electron energy-loss spectra obtained from the Pt_1-Co_3O_4 and Pt/Co_3O_4 materials are presented in **Figure 2**a. Pronounced peaks at H780 and 795 eV are characteristic of L_3 and L_2-shell ionization edges in Co, respectively.[17] It is evident that approximately a third of the Co present exists as Co^{2+} in a tetrahedral coordination to oxygen and two-thirds exist as Co^{3+} in an octahedral oxygen environment in the SAC. [18] In the octahedral coordination, the tetrahedral environment splits the Co 3d states into three t_{2g} and two e_g levels. The propor-tion of tetrahedral/octahedral species present in the Pt_1-Co_3O_4 catalyst is notably higher than that observed in the Pt/Co_3O_4, indicating that there is a strong interaction between the single-atom Pt sites and Co_3O_4 supports in the Pt_1-Co_3O_4 catalyst, which in turn, would facilitate the formation of Co^{3+} species. These results can be supported by XPS experiments presented in Figure 2b. The asymmetrical Co $2p_{3/2}$ region can be decon-voluted into two components centered at binding energies of 779.4 and 780.7 eV, characteristic of surface Co^{2+} and Co^{3+} spe-cies, respectively.[19] The proportion of Co^{3+}/Co^{2+} in each catalyst was subsequently quantified and the ratios were determined to be 1.71, 1.97, and 2.42 for the Co_3O_4, Pt/Co_3O_4, and Pt_1-Co_3O_4 catalysts, respectively. Furthermore, the XPS spectra of samples with different Pt loadings indicated that the ratio of Co^{3+}/Co^{2+} was enhanced with the increasing of Pt content, attributing to the support–metal strong interaction in these SACs (Figure S6, Supporting Information). The Co^{3+} species is clearly dominant, which is unsurprising given that this species is known to be pivotal in low-temperature oxidation reactions over Co_3O_4 cata-lysts.[13] According to previous reports, the Pt^0 species were seen as the preponderant active sites compared with Pt^{2+} and Pt^{4+} species in VOC total oxidation.[4] In this work, a higher

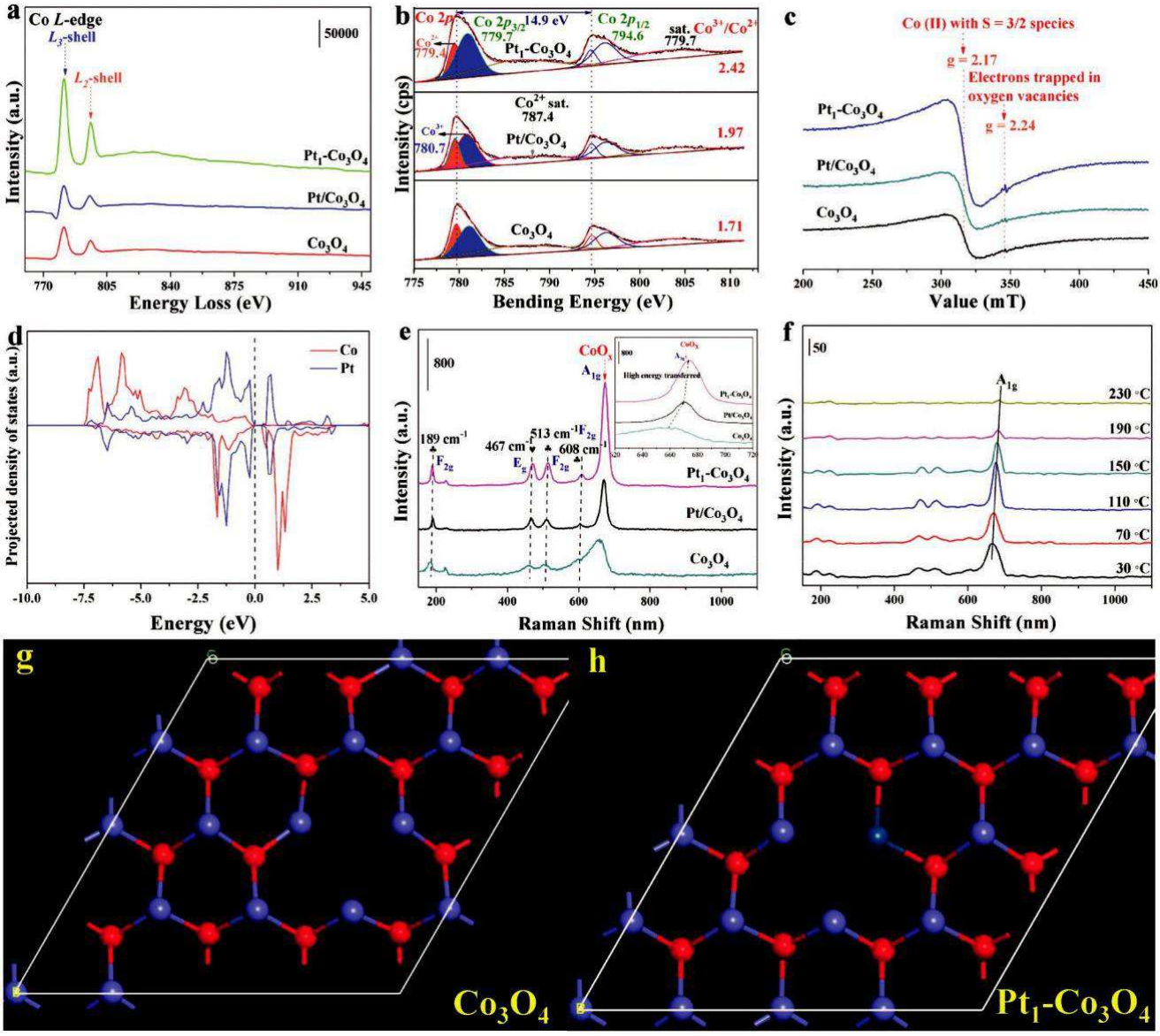

Figure 2. a) Electron energy-loss spectroscopy (EELS) of Co atom; b) Co 2p XPS spectra of samples; c) Electron paramagnetic resonance (EPR) spectra of samples; d) Projected density of states of Co and Pt 3d orbital on the defective Pt_1-Co_3O_4 surface. (All energies referenced to the Fermi level indicated by the dashed line); e) Laser Raman spectra of prepared samples; f) In situ Raman spectra of Pt_1-Co_3O_4 catalyst; g,h) The calculated formation energy of an oxygen vacancy over Co_3O_4 and Pt_1-Co_3O_4 samples (red, pink, and blue spheres represent O, Pt, and Co atoms, respectively).

ratio of Pt^0 species was detected over Pt_1-Co_3O_4 SAC material compared with supported Pt/Co_3O_4 sample (Figure S7, Supporting Information), which was ascribed to the strong interac-tion between Pt_1 active sites and Co_3O_4 support.[20] The strong interaction was further proved by Bader charge analysis based on the density functional theory (DFT) analysis, which revealed that the Pt atom carries a considerable positive charge (1.03 e). This interaction between Pt_1 active sites and Co_3O_4 support promotes the formation of oxygen vacancies and enhances the stability of single-atom catalyst.

Electron paramagnetic resonance (EPR) spectroscopy was subsequently used to probe the materials; see Figure 2c. Each of the catalysts exhibited a broad, intense resonance at $g = 2.17$ mT, which is characteristic of a Co(II) with S = 3/2 species.[21] According to a previous study, the quantity of high spin Co(II) species presenting in a given catalyst is propor-tional to the content of oxygen vacancies.[22] It is clearly evi-dent from Figure 2c, that the intensity of Co(II) peak in the Pt_1-Co_3O_4 catalyst is significantly greater than that observed for the Co_3O_4 and Pt/Co_3O_4 catalysts. Furthermore, an additional peak at $g = 2.24$ mT is observed in the EPR spectrum of the Pt_1-Co_3O_4 catalyst; the intensity of this peak in the spectra of the Co_3O_4 and Pt_1-Co_3O_4 materials is considerably smaller. This peak is considered to be characteristic of electrons trapped in oxygen vacancies.[19a,23] This could indicate that the Pt_1-Co_3O_4 catalyst possesses a higher proportion of oxygen vacancies than the Co_3O_4 and Pt/Co_3O_4 catalysts. This aligns with additional DFT calculations (Figure 2g,h), which reveal that the formation

energy for an oxygen vacancy (E_{vac}: energy needed to form one oxygen vacancy on the surface and half an oxygen molecule in the gas phase) on a Pt_1-Co_3O_4 (111) surface (1.52 eV) is much lower than that on a Co_3O_4 (111) surface (2.41 eV).

The Bader charge analysis confirmed that the formation of an oxygen vacancy leads to an increased electron density on the Pt (0.4 e). After adsorption of methanol and O_2, the electron on the Pt atoms decreased by 0.2 and 0.5 e, respectively. It is likely that the Pt atoms exhibit a stronger adsorption capacity on the defec-tive surface than that on the Co_3O_4 (111) and Pt_1-Co_3O_4 (111) sur-faces. To further investigate this conclusion, the density of states (DOS) of the Pt and Co 3d orbital was compared, as displayed in Figure 2d. The Pt atom with a higher occupied orbital exhibits a stronger affinity to methanol and O_2, which can be ascribed to the decreased filling of adsorbate–metal antibonding states. Thus, methanol and O_2 molecules are more likely to coadsorb onto a defective Pt_1-Co_3O_4 surface and the adsorption capacity is greatly enhanced by the oxygen vacancies. Further evidence of this is provided by O_2-temperature-programmed desorption (TPD), methanol-TPD, and in situ Fourier transform infrared (FTIR) of methanol adsorption experiments, which are illus-trated in Figures S8–S10 (Supporting Information), respectively.

The optimized configurations of methanol and O_2 over the Pt_1-Co_3O_4 (111) surface are presented in Figure S11 and Table S2 (Supporting Information). The calculated adsorption energy of methanol is 0.03 eV. The O atom of the methanol molecule bonds to the Pt atom and the distance between Pt and O atoms is calculated to be 2.78 Å. O_2 molecules can also adsorb onto Pt sites with an exothermic energy of 0.3 eV and exhibit a Pt O bond length of 2.13 Å. In contrary, the adsorption energy of methanol and O_2 onto the Co_3O_4 (111) surface is 0.91 and 0.49 eV, respectively (Figure S12, Supporting Information). The adsorption of methanol and O_2 on the defective Pt_1-Co_3O_4 (111) surface was subsequently investigated (Figure S13, Sup-porting Information). With this catalyst, it was determined that methanol adsorbs onto a Pt site with an energy of 1.48 eV and the resultant Pt O bond length was calculated to be 2.08 Å. This notable enhancement is likely to be attributed to the OH group in the methanol partaking in hydrogen bonding interac-tions with the lattice oxygen species. The adsorption energy of O_2 over this catalyst was calculated to be 0.66 eV. As such, it can be concluded that increasing the quantity of oxygen vacan-cies in the catalyst greatly enhances both the methanol and O_2 adsorption significantly, which is obviously very well important for total oxidation catalysts.[4]

In the Pt_1-Co_3O_4 material, we have confirmed that the Pt atoms instigate the charge imbalance and increase the pro-portion of oxygen vacancies in the catalyst. In Figure 2e, the Pt_1-Co_3O_4 catalyst, which exhibits AB_2O_4 structure (where A and B represent Co^{2+} and Co^{3+}, respectively), consists of five Raman-active modes: A_{1g}, E_g, and three F_{2g} modes, centered at 675, 467, 513, 189, and 608 cm^{-1}, respectively.[24] The F_{2g} and E_g modes suggest that there are different motions in the tetra-hedral sites (CoO_4 unit); the F_{2g} mode at 189 cm^{-1} is assigned to a complete translation of the CoO_4 unit within the lattice. The A_{1g} mode can be attributed to the octahedral CoO_6 sites of crystalline Co_3O_4 phase. Interestingly, when the spectra of the Co_3O_4 and Pt/Co_3O_4 modes were investigated, the posi-tions of all recorded Raman peaks of Pt_1-Co_3O_4 shift to higher frequencies and the intensity of A_{1g} symmetry increases, which is indicative of defects in the crystal structure. Analysis of in situ Raman spectra, the intensity of the peak at about 665 cm^{-1}, characteristic of Co O bond vibration, decreases in the spectrum of the Pt/Co_3O_4 as temperature increases from 0 to 230 °C; see Figure S14 (Supporting Information). This is likely to be attributed to a change in the crystalline phase as the temperature is increased. Interestingly, in the experiment over the Pt_1-Co_3O_4 catalyst, this peak goes through a max at 110 °C; see Figure 2f. This suggests that at this temperature, the pres-ence of oxygen vacancies in the catalysts is at its highest, which in turn, indicates that the electron transfer from Pt to Co is at its most efficient at this temperature.

2.3. Catalytic Performance of Prepared Materials

Methanol was used as a substrate to assess the catalytic potential of the Pt_1-Co_3O_4 SAC. The results from these ini-tial experiments are displayed in **Figure 3** and **Table 1**. It was determined that over the Pt_1-Co_3O_4 catalyst, the complete oxida-tion of methanol into CO_2 and H_2O could be achieved at only 110 °C (Figure 3a). The reaction rate and turnover frequency of Pt-based catalysts prepared in this study were subsequently assessed (Figures S15 and S16, Supporting Information). A reaction rate of 0.013 mol g_{Pt}^{-1} s^{-1} was determined for the Pt_1-Co_3O_4 catalyst at 70 °C, which was over four times higher than that observed over the Pt/Co_3O_4 catalyst (0.03 mol g_{Pt}^{-1} s^{-1}; Figure 3b and Figure S15, Supporting Information). The turnover frequencies (TOFs) exhibited by both catalysts were based on the Pt dispersion (Figure 3b and Figure S16, Supporting Infor-mation). The measurements indicate that the activity exhibited by each Pt site in Pt_1-Co_3O_4 catalyst was substantially higher at 70 °C, which to the best of our knowledge is higher than other catalysts previously reported for this reaction to date (Table S3, Supporting Information). These data were subsequently used to construct Arrhenius plots and establish activation energies (E_a) for methanol oxidation over each catalyst (Figure S17, Sup-porting Information). The activation energy of the single-site Pt_1-Co_3O_4 catalyst was substantially lower than that observed over the Pt/Co_3O_4 catalyst. Based on the observed activity of Pt_1-Co_3O_4 catalyst, we conduct the detailed correlation anal-ysis between catalytic performance and structure properties including: high specific surface area (Figure S18, Supporting Information, and Table 1), sufficient surface-bound hydroxyl species (Figure S19, Supporting Information), high quantity of lattice oxygen (Figures S20–S22, Supporting Information), supe-rior low-temperature reducibility (Figure S23, Supporting Infor-mation), high oxygen/methanol adsorption capacity (Figure S24, Supporting Information), and abundant oxygen vacancies (Figure S25, Supporting Information). As discussed, based on the experimental and theoretical studies conducted in this work, we consider that the significant increase in the quantity of oxygen vacancies over the Pt_1-Co_3O_4 catalyst is likely to be the most crucial factor, the electron transfer over the oxygen vacancies reduces both the methanol adsorption energy and activation barriers for methanol oxidation, which was proposed to significantly enhance the dissociation of the C H bond in methanol decomposition reaction.

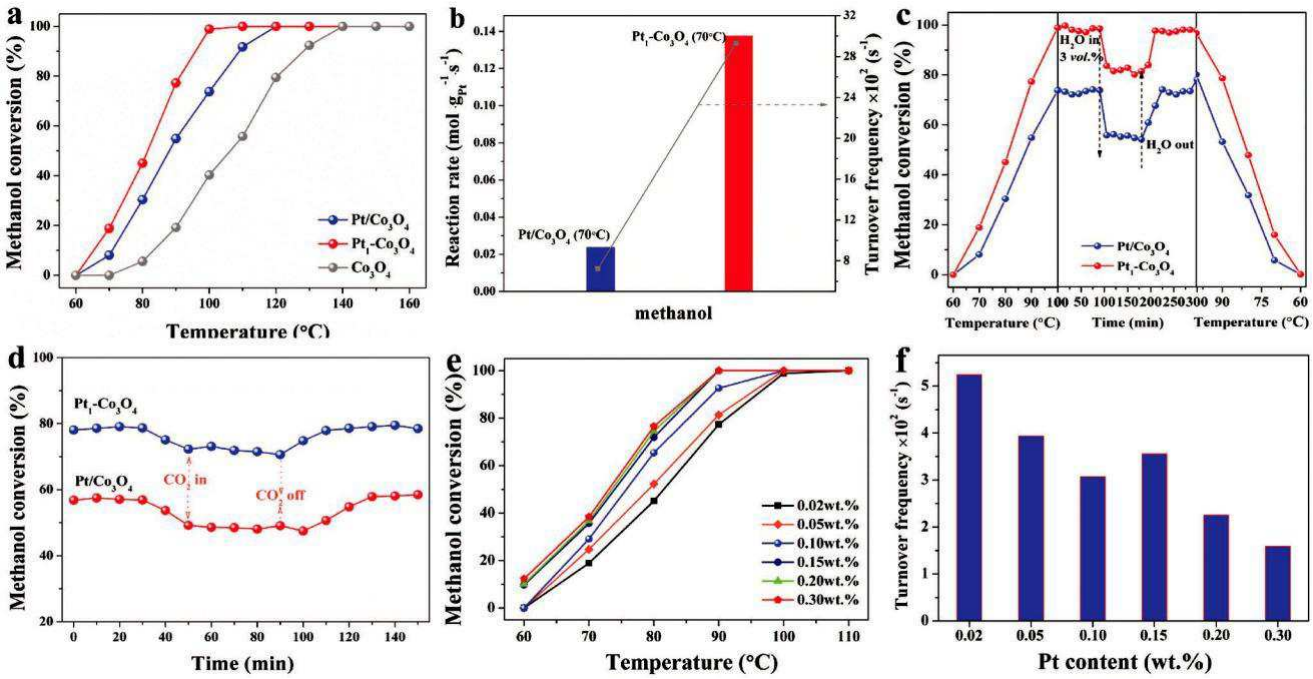

Figure 3. a) The performance of methanol oxidation over Pt-based materials; b) Reaction rate and turnover frequency for methanol oxidation over active catalysts at 70 °C; c) Catalytic stability for methanol oxidation of prepared catalysts; d) The CO_2 resistance of prepared catalysts during methanol oxidation at 90 °C; e) The light-off curves of methanol oxidation over Pt_1-Co_3O_4 catalyst with different Pt contents; f) Turnover frequency of methanol oxidation over various Pt_1-Co_3O_4 catalysts.

The stability test of prepared catalysts was subsequently performed. The resistance of water was examined by introducing 3 vol% of water vapor to the catalysts between a heating and cooling cycle (Figure 3c). After additional tests, notable losses in methanol conversion of H15.0 and 18.0% were observed over the Pt_1-Co_3O_4 and Pt/Co_3O_4 catalysts, respectively. Inter-estingly, however, the original activity was restored after only 30–45 min of stopping H_2O in the feed, suggesting that the reductions in activity were not indicative of permanent changes to the catalysts. In addition, the single-atom Pt_1-Co_3O_4 catalyst possesses a better CO_2 (5 vol%) resistance (Figure 3d), which can be attributed to the abundant oxygen vacancies around Pt active sites. The adequate oxygen vacancies around single-atom Pt provide sufficient adsorption sites for O_2 molecules during methanol oxidation, which restrains the competitive adsorp-tion of CO_2 and O_2 molecules to some extent. These catalysts are evidently highly stable, which was supported by in situ X-ray diffraction (XRD) experiments (Figures S26 and S27, Supporting Information). In addition, the aberration corrected scanning transmission electron microscopy (ac-STEM) images of Pt_1-Co_3O_4 after oxidation reaction were performed in order to assess the aggregation of Pt active sites. As displayed in Figure S28 (Supporting Information), the Pt sites remain stable after the oxidation reactions at 150 and 200 °C; however, the Pt atoms aggregated to some extent when it involved in 250 °C. As such, the stability of SACs remains a challenge when involving VOC oxidation at high temperature.

We have explored the possibility and pushed to the limit activity of this catalyst in order to explore the application of SACs with higher metal loadings in VOC elimination. As shown in Figure 3e, the catalytic performance of prepared catalysts was promoted within 0.02–0.15 wt% of Pt con-tent for methanol oxidation; however, unobvious activity change can be found when further increasing the Pt con-tent to 0.20 or 0.30 wt% due to the formation of Pt nano-particles, identified by the hydrogen and oxygen titration

Table 1. Textural property and catalytic performance of prepared materials.

Sample	Pt content[a] [wt%]	Dispersion[b] [%]	S_{BET}[c] [$m^2\ g^{-1}$]	V_{pore}[d] [$cm^3\ g^{-1}$]	D_{pore}[e] [nm]	T_{50}[f] [°C]	T_{90}[f] [°C]	r_g[g] [mol $gPt^{-1}\ s^{-1}$]	TOF_{Pt}[h] × 10^2 [s^{-1}]
Co_3O_4	–	–	55.5	0.53	18.4	107	128	–	–
Pt/Co_3O_4	0.05	63.7	58.9	0.57	19.1	87	109	0.03	7.2
Pt_1-Co_3O_4	0.02	91.5	59.5	0.51	18.4	81	96	0.13	29.3

[a]Actual Pt content detected by ICP-OES; [b]The dispersion of Pt active sites measured by hydrogen and oxygen titration (HOT); [c]Specific surface area obtained at P/P_0 = 0.05–0.30; [d]Total pore volume estimated at P/P_0 = 0.99; [e]BJH pore diameter calculated from the adsorption branch; [f]Temperatures at which 50 and 90% conver-sion of methanol; [g]Reaction rate of methanol molecules transformed per Pt metal per unit time of various catalysts at 70 °C; [h]Turnover frequency based on the dispersion of Pt obtained at 70 °C.

experiment (Table S4, Supporting Information). We further calculated the turnover frequency of prepared materials at 62 °C (conversion lower than 20%), as shown in Figure 3f. The TOF of Pt sites maintained at around 0.03–0.05 s^{-1} within 0.02–0.15 wt% of Pt and declined when Pt loading increased (0.0225 s^{-1} for 0.20 wt% P_1-Co_3O_4; 0.0159 s^{-1} for 0.30 wt% P_1-Co_3O_4). Above results indicate that the actual active sites of these Pt_1-Co_3O_4 catalysts are Pt_1 single atoms. The Pt loading of 0.15 wt% is the limit of single-atom Pt_1-Co_3O_4 cata-lyst prepared by this coprecipitation method in this work, over which the complete oxidation of 700 ppm methanol could be achieved at only 90 °C and with a 0.0356 s^{-1} TOF at 62 °C.

2.4. Insight on the Atomic-Level Mechanism

In this work, the low-concentration VOC oxidation over the single-atom materials follows a first-order reaction, which is ascribed to the excess of oxygen in the reaction system and the reaction rate is only proportional to the first power of VOC concentration. A detailed understanding of the oxidative surface mechanisms for VOCs over SACs would be incredibly beneficial from a catalyst design perspective.[25] For this reason, a series of in situ diffuse reflectance infrared Fourier transform spectros-copy (DRIFTS) experiments were conducted over the Pt_1-Co_3O_4 and Pt/Co_3O_4 catalysts, in an attempt to derive information regarding the intermediate products formed during the reac-tion (**Figure 4**a,b). The spectra of both catalysts consist of bands characteristic of C H bond vibrations (2892 cm^{-1}) and surface-bound hydroxyl species (3050 and 1431/1422 cm^{-1}).[26] The peaks centered at 1257/1230 cm^{-1} are attributed to the vibra-tion of methoxy species.[26c] Interestingly, an additional band is observed at 1494 cm^{-1} in the spectrum of Pt_1-Co_3O_4, which is typically characteristic of a symmetric carbonyl groups.[27] It is likely that after coadsorption of CH_3OH and O_2, the OH group of CH_3OH molecule can dissociate, leading to the formation

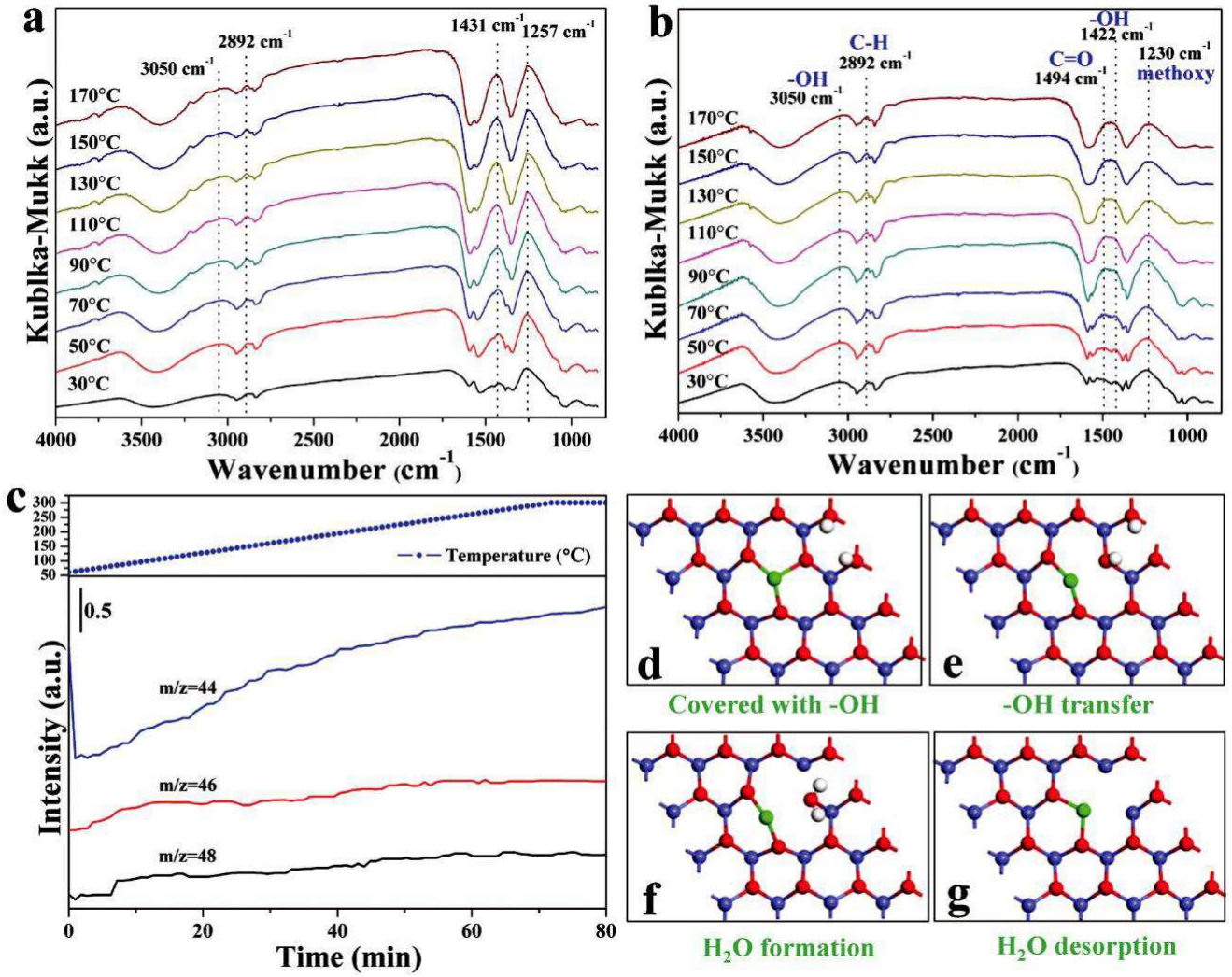

Figure 4. a,b) In situ DRIFTS of methanol oxidation over Pt/Co_3O_4 and Pt_1-Co_3O_4 catalysts; c) $^{18}O_2$ isotopic exchange studies of Pt_1-Co_3O_4 for methanol oxidation; d–g) The geometries in the process of new oxygen vacancy formation (only the top two layers are given in order to show clearly; red, green, white, and blue spheres represent O, Pt, H, and Co atoms, respectively).

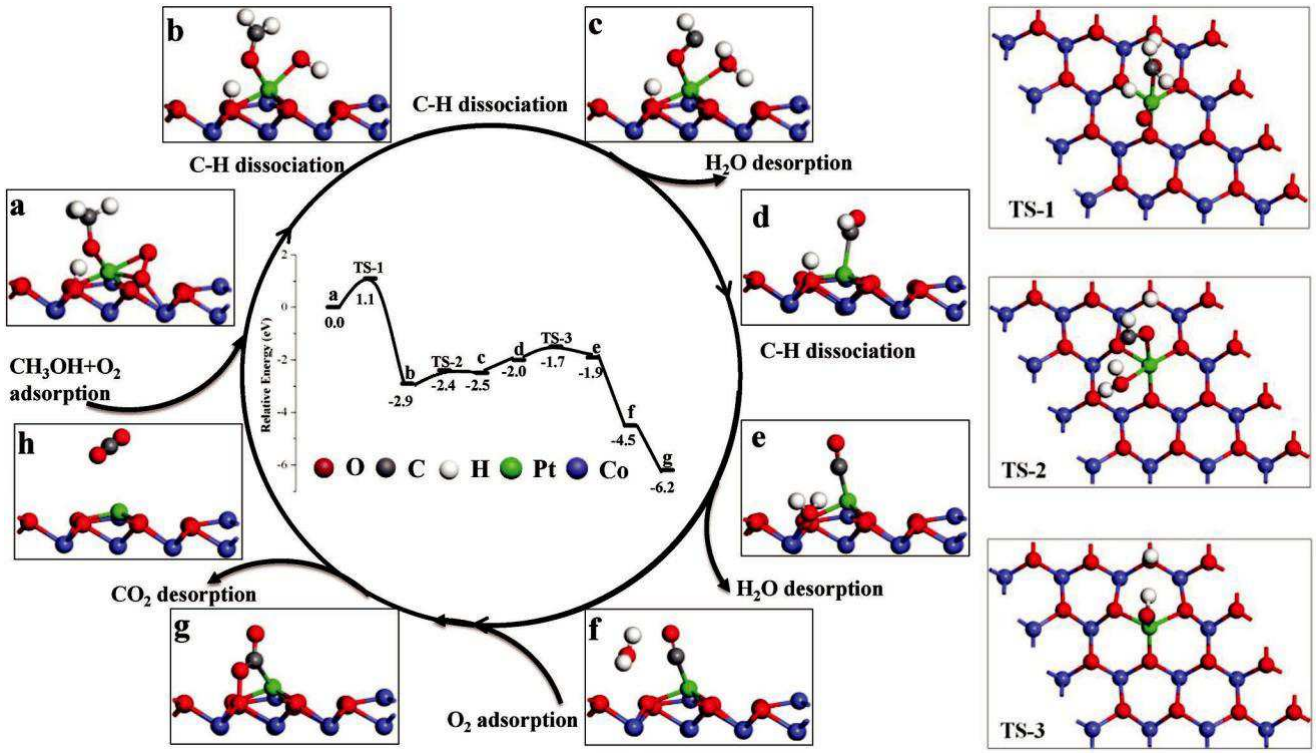

Figure 5. Proposed reaction pathways and the corresponding transition states for methanol oxidation over Pt_1-Co_3O_4 catalyst.

of Pt-methoxyl species. The oxygen vacancies regeneration and electron transfer over Pt atoms accelerate the C H bond activa-tion over methoxyl species, which go through the formaldehyde as intermediate and then oxidized into H_2O and CO_2.

The ^{18}O isotope tracer technique was introduced to inves-tigate the lattice oxygen transformation. Figure 4c displays the products containing isotopic species ($C^{18}O_2$, $C^{16}O\ ^{18}O$, and $C^{16}O_2$) during methanol oxidation. All these species showed the temperature-dependent variation. The $C^{16}O_2$ species took a vigorous increasing after the reaction beginning, mean-while, the signal of $C^{16}O^{18}O$ and $C^{18}O_2$ species grew tardily during the oxidation reaction. This phenomenon provides the evidence that lattice oxygen is the primary active oxygen species during methanol elimination over Pt_1-Co_3O_4 catalyst. It is widely accepted that the process of oxygen vacancies regeneration provides abundance of hydroxyl groups for sam-ples, which plays a significant role in intermediates decom-position.[28] As such, some additional theoretical experiments were conducted in order to investigate how the regenera-tion of oxygen vacancies on the surface of the Pt_1-Co_3O_4 was affected by the presence of hydroxyl groups (Figure 4d–g). The Pt_1-Co_3O_4 surface was first saturated with hydroxyl groups (O_aH or O_bH); evidence for their introduction is displayed in Figure 4d. For a H atom to migrate from O_b to a lattice oxygen atom bonded to Pt ($O_{Pt}H$), the energy barrier was determined to be 0.3 eV (Figure 4e). This allows for the subsequent migra-tion of an additional H atom from a lattice oxygen species to the $O_{Pt}H$, resulting in the production of a H_2O molecule (Figure 4f). This process was determined to be endothermic (0.95 eV). The sequential desorption of the H_2O on the surface of the Pt_1-Co_3O_4 catalyst leads to the liberation of the lattice oxygen sites (Figure 4g).

Based on the DFT calculations, a catalytic cycle for the oxidation of CH_3OH and the corresponding transition states over the Pt_1-Co_3O_4 catalyst is proposed in **Figure 5**. First of all, a surface phase diagram was provided for Pt_1-Co_3O_4 as the surface can be with an oxygen defect or adsorption phase. The calculated surface free energies of the three possible terminations are shown in Figure S29 (Supporting Infor-mation). The temperature of T = 600 K corresponds to the annealing temperature employed in our experiment. When

$\propto_O$ becomes extremely low (lower than 1.46 eV), the Pt_1-$Co_{3n}O_{4n-1}$ surface is the most stable structure. Accordingly, Pt_1-Co_3O_4 surface with an oxygen vacancy is used to inves-tigate the oxidation of methanol in this work. After coad-sorption of the CH_3OH and O_2, the OH group of CH_3OH molecule can dissociate ($CH_3OH \rightarrow CH_3O + H$), leading to the formation of Pt-methoxyl species and H atom required for the formation of the $O_{3c}H$ species (Figure 5a). In the absence of Pt, over the Co_3O_4 (111) surface, a significantly higher energy barrier is required for this reaction pathway (0.2 eV). O_2 activation over the Pt_1-Co_3O_4 (111) surface leads to the formation of a peroxide-type O_2^{2-} species. One oxygen atom of O_2 molecule fills the oxygen vacancy and the other oxygen atom binds to an adjacent Pt atom. The Pt O and O O bonds lengths were determined to be 2.09 and 1.40 Å, respectively. With the assistance of the active oxygen species O_2^{2-}, the methoxyl species partake in a C H bond cleavage, leaving a surface-bound CH_2O species ($CH_3O \rightarrow CH_2O + H$), the energy barrier of which was determined to be 1.14 eV

Table 2. The forward and backward rates of each elementary reaction step for methanol oxidation at 375 K.

Reaction steps	Forward rate [s^{-1}]	Backward rate [s^{-1}]	Overall reaction rate [s^{-1}]	Degree of rate control
$CH_3OH + * \rightarrow CH_3O*H$	5.29×10^{-2}	5.14×10^{-2}	1.44×10^{-3}	1.18×10^{-12}
$CH_3O*H + O_2 \rightarrow CH_3O*HO_2$	1.39×10^{9}	1.39×10^{9}	2.87×10^{-3}	7.76×10^{-13}
$CH_3O*HO_2 \rightarrow CH_2O*HO_2H$	1.44×10^{-3}	2.82×10^{-50}	1.44×10^{-3}	9.96×10^{-1}
$CH_2O*HO_2H \rightarrow CHO*HOH_2O$	2.10×10^{-3}	6.63×10^{-4}	1.44×10^{-3}	7.38×10^{-10}
$CHO*HOH_2O \rightarrow CHO*HO + H_2O$	1.44×10^{-3}	0	1.44×10^{-3}	3.41×10^{-10}
$CHO*HO \rightarrow HCO*HO$	7.19×10^{3}	7.19×10^{3}	1.44×10^{-3}	7.38×10^{-10}
$HCO*HO \rightarrow CO*H_2O$	1.44×10^{-3}	8.37×10^{-10}	1.44×10^{-3}	3.70×10^{-3}
$CO*H_2O \rightarrow H_2O + CO*$	1.44×10^{-3}	0	1.44×10^{-3}	2.12×10^{-9}
$CO* + O_2 \rightarrow CO_2*O$	1.44×10^{-3}	1.98×10^{-61}	1.44×10^{-3}	9.11×10^{-13}
$CO_2*O \rightarrow CO_2 + *$	1.44×10^{-3}	0	1.44×10^{-3}	0

(1.37 eV on Co_3O_4 (111) surface). The surface-bound hydrogen atoms can also interact with the O_2^{2-} species, leading to the formation of OH groups (Figure 5b). Through interaction with these surface hydroxyls, the CH_2O interme-diate species can undergo a sequential C H dissociation to produce CHO and H_2O. The calculated activation barrier for this step over the Pt_1-Co_3O_4 (111) surface is 0.44 eV, but is significantly higher in the absence of Pt, 1.78 eV. The CHO group subsequently binds to the Pt atom to form a Pt OCH species (Figure 5c). Following this, H_2O desorbs and Pt OCH undergoes a geometric distortion to form Pt CHO (Figure 5d). This process is endothermic (0.46 eV). The C H bond of CHO can then undergo further decomposi-tion (CHO + OH $\rightarrow$ CO + H_2O) with an energy barrier of 0.54 eV and the hydrogen atom adsorbs onto another $O_{3c}H$ group to form water (Figure 5e). Water desorbs with an energy of 0.35 eV, leaving only the CO molecule bound to a Pt atom and an oxygen vacancy on the surface (Figure 5f). Finally, an additional O_2 molecule adsorbs to the oxygen vacancy and dis-sociates, providing the additional oxygen atom required for oxidizing CO to CO_2. This step releases the energy of 2.65 eV (Figure 5g). The CO_2 subsequently desorbs, releasing heat (1.67 eV) and the surface of the Pt_1-Co_3O_4 SAC returns to ini-tial state without oxygen (Figure 5h). As such, the surfaces of the oxide particles are covered with (OH) formed by the dis-sociative chemisorption of water.[29] Following, a microkinetics simulation has been carried out by MKMCXX software.[30] In the whole catalytic reaction cycle, the energy barrier of the recovery of Pt_1-Co_3O_4 surface is only 0.3 eV, which is easy to achieve. Thus, we ignored the process of surface recovery and assumed that the reaction cycle finished after the desorption of CO_2. The initial concentration of CH_3OH and O_2 is set as 2:3, and the pressure is set as 1 atm. The forward and back-ward rates of each elementary reaction step of methanol oxi-dation at 375 K are shown in **Table 2**. It can be seen that the step of $CH_3O*HO_2 \rightarrow CH_2O*HO_2H$ has the largest degree of rate control value, indicating that the cleavage of C H bond of (CH_3O*) influences the reaction the most. It is related with the largest energy barrier of this step in the whole reaction cycle. The corresponding surface coverage results show that CH_3O*H and CH_3O*HO_2 are predominate surface species (73.1 and 26.4%), which attributes to the weak adsorption of O_2. The calculated apparent activation energy decreases with the increase of temperature, and the apparent activation energy for CH_3OH oxidation at 375 K is 55.1 kJ mol^{-1}.

3. Conclusion

Through a combination of theoretical and experimental inves-tigation, a detailed description for the geometric and electronic structure of a Pt_1-Co_3O_4 single-atom catalyst was derived. This catalyst was determined to consist of isolated single Pt atoms anchored to Co_3O_4 (111) planes, which occupied positions on the Co^{2+} atoms. The Pt_1-Co_3O_4 exhibited an excellent activity for the oxidation of methanol. One-third of the Co atoms in this catalyst were determined to exist as Co^{2+} in a tetrahedral coor-dination to oxygen; the remaining Co atoms were present as Co^{3+} in an octahedral oxygen environment. The Pt sites, which had high occupied electronic states, exhibited a strong affinity for the 3d orbital of adjacent Co atoms, resulting in significant electron transfer from Pt to Co, ultimately, increasing the pro-portion of oxygen vacancies present on the catalysts surface. Regeneration of these oxygen vacancies was determined to promote the coadsorption of methanol and O_2, leading to an increase in the rate of C H bond dissociation. DFT calcula-tions revealed that the electron transfers reduced the activation barriers for methanol oxidation. The discovery of this single-atom Pt catalyst highlights that single-site heterogeneous cat-alysts can be exceptionally effective for the oxidation of VOCs and provides a method for reducing the cost of noble-metal catalysts in industrial applications.

4. Experimental Section

All experimental details can be found in the Supporting Information.

Supporting Information

Supporting Information is available from the Wiley Online Library or from the author.

Acknowledgements

Y.J., X.B.F., and J.L.D. contributed equally to this work. This work was supported financially by the National Natural Science Foundation of China (21677114, 21876139, 21477095) and the National Key Research and Development Program (2016YFC0204201). The valuable comments and suggestions from Prof. Graham Hutchings in Cardiff University are much appreciated.

Conflict of Interest

The authors declare no conflict of interest.

Keywords

developed oxygen vacancies, DFT calculations, mechanism, single-atom catalysts, VOC low-temperature oxidation

[1] a) C. He, J. Cheng, X. Zhang, M. Douthwaite, S. Pattisson, Z. P. Hao, *Chem. Rev.* **2019**, *119*, 4471; b) Z. Y. Jiang, C. W. Chen, M. D. Ma, Z. Guo, Y. K. Yu, C. He, *Catal. Sci. Technol.* **2018**, *8*, 5933.

[2] C. G. Li, C. Paris, J. Martínez-Triguero, M. Boronat, M. Moliner, A. Corma, *Nat. Catal.* **2018**, *1*, 547.

[3] a) S. Royer, D. Duprez, F. Can, X. Courtois, C. Batiot-Dupeyrat, S. Laassiri, H. Alamdari, *Chem. Rev.* **2014**, *114*, 10292; b) C. B. Zhang, F. D. Liu, Y. P. Zhai, H. Ariga, N. Yi, Y. C. Liu, K. Asakura, M. Flytzani-Stephanopoulos, H. He, *Angew. Chem., Int. Ed.* **2012**, *51*, 9628.

[4] a) C. He, Z. Y. Jiang, M. D. Ma, X. D. Zhang, M. Douthwaite, J. W. Shi, Z. P. Hao, *ACS Catal.* **2018**, *8*, 4213; b) Z. Y. Jiang, C. He, N. F. Dummer, J. W. Shi, M. J. Tian, C. Y. Ma, Z. P. Hao, S. H. Taylor, M. D. Ma, Z. X. Shen, *Appl. Catal., B* **2018**, *226*, 220.

[5] a) J. Zhang, L. Wang, B. S. Zhang, H. S. Zhao, U. Kolb, Y. H. Zhu, L. M. Liu, Y. Han, G. X. Wang, C. T. Wang, D. S. Su, B. C. Gates, F. S. Xiao, *Nat. Catal.* **2018**, *1*, 540; b) H. B. Zhang, G. G. Liu, L. Shi, J. H. Ye, *Adv. Energy Mater.* **2018**, *8*, 1701343.

[6] A. Q. Wang, J. Li, T. Zhang, *Nat. Rev. Chem.* **2018**, *2*, 65.

[7] a) J. Jones, H. F. Xiong, A. T. DeLaRiva, E. J. Peterson, H. Pham, S. R. Challa, G. S. Qi, S. Oh, M. H. Wiebenga, X. I. P. Hernández, Y. Wang, A. K. Datye, *Science* **2016**, *353*, 150; b) H. X. Xu, D. J. Chen, D. P. Cao, X. C. Zeng, *Nat. Catal.* **2018**, *1*, 339; c) W. Zhang, W. T. Zheng, *Adv. Funct. Mater.* **2016**, *26*, 2988.

[8] J. C. Liu, Y. G. Wang, J. Li, *J. Am. Chem. Soc.* **2017**, *139*, 6190.

[9] a) B. T. Qiao, A. Q. Wang, X. F. Yang, L. F. Allard, Z. Jiang, Y. T. Cui, J. Y. Liu, J. Li, T. Zhang, *Nat. Chem.* **2011**, *3*, 634; b) A. J. Therrien, A. J. R. Hensley, M. D. Marcinkowski, R. Q. Zhang, F. R. Lucci, B. Coughlin, A. C. Schilling, J. S. McEwen, E. C. H. Sykes, *Nat. Catal.* **2018**, *1*, 192; c) L. Nie, D. H. Mei, H. F. Xiong, B. Peng, Z. B. Ren, X. I. P. Hernandze, A. DeLaRiva, M. Wang, M. H. Engelhard, L. Kovarik, A. K. Datye, Y. Wang, *Science* **2017**, *358*, 1419; d) Z. L. Zhang, Y. H. Zhu, H. Asakura, B. Zhang, J. G. Zhang, M. X. Zhou, Y. Han, T. Tanaka, A. Q. Wang, T. Zhang, N. Yan, *Nat. Commun.* **2017**, *8*, 16100.

[10] a) D. H. Deng, X. Q. Chen, L. Yu, X. Wu, Q. F. Liu, Y. Liu, H. X. Yang, H. F. Tian, Y. F. Hu, P. P. Du, R. Si, J. H. Wang, X. J. Cui, H. B. Li, J. P. Xiao, T. Xu, J. Deng, F. Yang, P. N. Duchesne, P. Zhang, J. G. Zhou, L. T. Sun, J. Q. Li, X. L. Pan, X. H. Bao, *Sci. Adv.* **2015**, *1*, e1500462; b) S. H. Sun, G. X. Zhang, N. Gauquelin, N. Chen, J. G. Zhou, S. L. Yang, W. F. Chen, X. B. Meng, D. S. Geng, M. N. Banis, R. Y. Li, S. Y. Ye, S. Knights, G. A. Botton, T. K. Sham, X. L. Sun, *Sci. Rep.* **2013**, *3*, 1775.

[11] P. P. Hu, Z. W. Huang, Z. Amghouz, M. Makkee, F. Xu, F. Kapteijn, A. Dikhtiarenko, Y. X. Chen, X. Gu, X. F. Tang, *Angew. Chem., Int. Ed.* **2014**, *53*, 3418.

[12] a) F. Dvorˇák, M. F. Camellone, A. Tovt, N. D. Tran, F. R. Negreiros, M. Vorokhta, T. Skála, I. Matolínová, J. Myslivecek, V. Matolín, S. Fabris, *Nat. Commun.* **2016**, *7*, 10801; b) J. Y. Liu, *ACS Catal.* **2017**, *7*, 34.

[13] X. W. Xie, Y. Li, Z. Q. Liu, *Nature* **2009**, *458*, 746.

[14] Y. X. Liu, H. X. Dai, J. G. Deng, S. H. Xie, H. G. Yang, W. Tan, W. Han, Y. Jiang, G. S. Guo, *J. Catal.* **2014**, *309*, 408.

[15] L. C. Liu, U. Díaz, R. Arenal, G. Agostini, P. Concepción, A. Corma, *Nat. Mater.* **2017**, *16*, 132.

[16] a) Y. R. Zhu, Z. An, J. He, *J. Catal.* **2016**, *341*, 44; b) L. DeRita, S. Dai, K. Lopez-Zepeda, N. Pham, G. W. Graham, X. Q. Pan, P. Christopher, *J. Am. Chem. Soc.* **2017**, *139*, 14150; c) K. L. Ding, A. Gulec, A. M. Johnson, N. M. Schweitizer, G. D. Stucky, L. D. Mark, P. C. Stair, *Science* **2015**, *350*, 189.

[17] R. M. Wang, C. M. Liu, H. Z. Zhang, C. P. Chen, L. Guo, H. B. Xu, S. H. Yang, *Appl. Phys. Lett.* **2004**, *85*, 2080.

[18] H. A. E. Hagelin-Weaver, G. B. Hoflund, D. M. Minahan, G. N. Salaita, *Appl. Surf. Sci.* **2004**, *235*, 420.

[19] a) B. F. Chen, F. B. Li, Z. J. Huang, G. Q. Yuan, *Appl. Catal., B* **2017**, *200*, 192; b) X. X. Wang, D. A. Cullen, Y.-T. Pan, S. Hwang, M. Y. Wang, Z. X. Feng, J. Y. Wang, M. H. Engelhard, H. G. Zhang, Y. H. He, Y. Y. Shao, D. Su, K. L. More, J. S. Spendelow, G. Wu, *Adv. Mater.* **2018**, *30*, 1706758.

[20] a) I. Ro, J. Resasco, P. Christopher, *ACS Catal.* **2018**, *8*, 7368; b) M. Y. Mao, H. Q. Lv, Y. Z. Li, Y. Yang, M. Zeng, N. Li, X. J. Zhao, *ACS Catal.* **2016**, *6*, 418.

[21] J. G. Mcalpin, Y. Surendranath, M. Dinca, T. A. Stich, S. A. Stoian, W. H. Casey, D. G. Nocera, R. D. Britt, *J. Am. Chem. Soc.* **2010**, *132*, 6882.

[22] K. Deori, S. Deka, *CrystEngComm* **2013**, *15*, 8465.

[23] J. B. Priebe, M. Karnahl, H. Junge, M. Beller, D. Hollmann, A. Bruckner, *Angew. Chem., Int. Ed.* **2013**, *52*, 11420.

[24] a) S. P. Mo, Q. Zhang, S. D. Li, Q. M. Ren, M. Y. Zhang, Y. D. Xue, R. S. Peng, H. L. Xiao, Y. F. Chen, D. Q. Ye, *ChemCatChem* **2018**, *10*, 3012; b) B. Rivas-Murias, V. Salgueiriño, *J. Raman Spectrosc.* **2017**, *48*, 837.

[25] X. L. Zou, Z. B. Rui, S. Q. Song, H. B. Song, *J. Catal.* **2016**, *338*, 192.

[26] a) R. D. Zhang, D. J. Shi, N. Liu, Y. Cao, B. H. Chen, *Appl. Catal., B* **2014**, *146*, 79. b) Y. T. Lai, T. C. Chen, Y. K. Lan, B. S. Chen, J. H. You, C. M. Yang, N. C. Lai, J. H. Wu, C. S. Chen, *ACS Catal.* **2014**, *4*, 3824; c) S. K. Matam, R. F. Howe, A. Thetford, C. R. A. Catlow, *Chem. Commun.* **2018**, *54*, 12875.

[27] C. S. Chen, Y. T. Lai, T. C. Chen, C. H. Chen, J. F. Lee, C. W. Hsu, H. M. Kao, *Nanoscale* **2014**, *6*, 12644.

[28] F. Zasada, J. Janas, W. Piskorz, M. Gorczynska, Z. Sojka, *ACS Catal.* **2017**, *7*, 2853.

[29] C. Liu, Q. X. Ma, H. He, G. Z. He, J. Z. Ma, Y. C. Liu, Y. Wu, *Environ. Sci.: Nano* **2017**, *4*, 2388.

[30] I. A. W. Filot, R. A. van Santen, E. J. M. Hensen, *Angew. Chem., Int. Ed.* **2014**, *53*, 12746.